

Microstructural investigation of four kinds of γ' -Fe₄N nitrides in ion-nitrided pure iron

Z.Q. Liu^{a)}

Shenyang National Laboratory for Materials Science, Institute of Metal Research, Chinese Academy of Sciences, Shenyang 110016, China, and Institute of Materials and Technology, Dalian Maritime University, Dalian 116026, China

Z.K. Hei

Institute of Materials and Technology, Dalian Maritime University, Dalian 116026, China

D.X. Li

Shenyang National Laboratory for Materials Science, Institute of Metal Research, Chinese Academy of Sciences, Shenyang 110016, China

(Received 21 December 2001; accepted 15 July 2002)

Conventional and high-resolution electron microscopies were used to investigate the microstructure and precipitation mechanism of four kinds of γ' -Fe₄N nitrides, formed at the surface during nitriding of polycrystalline pure iron sheet. γ' nitrides in the top columnar compound layer were thin plates (3–12 nm), which precipitated from ϵ -Fe₂₋₃N grains with orientation relationship of $(1\bar{1}1)\gamma'//\langle 0001\rangle\epsilon$ and $[011]\gamma'//[1\bar{2}10]\epsilon$. Those in the transition compound layer remained as equiaxed grains (1–1.5 μm), which grew from the α -Fe substrate during nitriding. In the diffusion layer, striated γ' nitrides nucleated from α'' -Fe₁₆N₂ nitrides with orientation relationship of $(100)\gamma'//\langle 1\bar{1}0\rangle\alpha''$ and $[011]\gamma'//[111]\alpha''$, while unstriated γ' nitrides precipitated from the α -Fe substrate with the orientation relationship of $(100)\gamma'//\langle 1\bar{1}0\rangle\alpha$ and $[011]\gamma'//[111]\alpha$.

I. INTRODUCTION

Nitriding of iron and steel has received considerable interest due to the beneficial surface properties it produces. It was concluded that the nitrided surface layer had good resistance to wear, corrosion, and fatigue. This process therefore has been widely applied in industry as an important method of surface modification.^{1–5} The microstructure of the nitrided layer has attracted much attention because of its important influence on the surface properties of the nitrided workpiece. Extensive investigations have been done on this subject with different methods.^{6,7} The microstructures of the nitrided layer are different according to various nitriding methods and procedures. In the general case, the nitrided layer consists of a compound layer and a diffusion layer, and the compound layer is divided into columnar and transition sublayers, which could be viewed cross-sectionally by optical microscopy^{8,9} and transmission electron microscopy (TEM).^{10,11} The nitrided compound layer is composed of ϵ -Fe₂₋₃N (hexagonal close-packed structure,

hcp) and γ' -Fe₄N (face-centered cubic structure, fcc) nitrides, while in the diffusion layer γ' -Fe₄N and α'' -Fe₁₆N₂ (body-centered tetragonal structure, bct) nitrides precipitate from α -Fe substrate (body-centered cubic structure, bcc). It can be seen that the γ' -Fe₄N nitrides exist in not only the compound layer but also in the diffusion layer. Although the study of γ' -Fe₄N nitrides has been reported by many researchers,^{12–14} little attention has been paid to the γ' -Fe₄N nitrides in the surface-nitrided layer, where a gradient of nitrogen concentration exists from the surface to the interior. The present paper is focused on the γ' -Fe₄N nitrides in the different nitrided sublayers. The microstructures and nitride transformations of four kinds of γ' -Fe₄N nitrides in ion-nitrided pure iron were studied systematically by using TEM and high-resolution electron microscopy (HREM).

II. EXPERIMENTAL

Rectangular samples (30 × 10 × 1.0 mm) were cut from a sheet of polycrystalline pure iron (<400 ppm impurities), and then the top surfaces were mirror polished before the nitriding treatment. The samples were nitrided at 823 K for 4 h in a gas mixture of NH₃ and 10% CH₃COCH₃ under a total pressure of 800–930 Pa and then were cooled within the ion-nitriding furnace to room temperature.

^{a)} Address all correspondence to this author.

Present address: Nanomaterials Laboratory, National Institute for Materials Science, 3-13 Sakura, Tsukuba 305-0003, Japan.
e-mail: LIU.zhiqian@nims.gp.jp

The nitrided samples were clipped with polishing holder, and the cross sections were polished and etched in Nital 1 pct. Thicknesses of nitrided layers were measured with light microscopy in bright field. Vickers diamond hardness was tested cross-sectionally to define the interface between compound and diffusion layers. The load used in the test was 19.6 N. The distinction between columnar and transition sublayers in the compound layer is difficult to make precisely with light microscopy because they are very thin. Thus, cross-sectional TEM specimens were prepared with the method illustrated in our previous papers, where the cross-sectional structures of nitrided A₃ steel⁹ and No. 45 steel¹¹ were presented. HREM observations were carried out on planar view specimens, which were prepared with the following procedures to show different layers: (i) Samples were mechanically polished from the nitrided surface to different thicknesses, from which the desired layer could be selected. This step was skipped for specimens of the top columnar layer and was utilized for specimens of the diffusion layer. For specimens of the middle transition layer, this step was replaced by ion milling at the last step. (ii) From the substrate side samples were then mechanically polished to 50 μm in thickness. (iii) 3-mm-diameter discs were punched from the samples and then were dimpled to 30 μm from the substrate side. (iv) Ion milling with argon ions under 4-kV accelerating voltage was employed finally to get TEM foils. To eliminate the mechanical damage at the top surfaces, all the dimpled discs were polished first from the substrate side and then from both sides at the last stage to get suitable thin areas. The time of single-side and double-side polishing could be adjusted by changing the parameters of ion milling. Both JEM-2000 and JEM-2010 (JEOL Ltd., Tokyo, Japan) electron microscopes were used for the TEM and HREM observations operated at an accelerating voltage of 200 kV. The nitrogen concentration depth profile was determined by electron beam probe analyzer.

III. RESULTS AND DISCUSSION

During ion-nitriding at high temperature, nitrogen atoms dissolve into the pure iron specimen through the surface. The concentration of nitrogen atoms increases from the surface to the interior with prolonged nitriding time. After the dissolved nitrogen atoms exceed the maximal solubility in ferrite, γ' nitrides nucleate at the surface and then grow both laterally and into the substrate as equiaxed grains. Eventually γ' grains coalesce with each other and establish a compound layer at the surface. The ϵ nitrides with a wider and higher content of nitrogen could nucleate at the top of the γ' layer under suitable nitriding potential. They grow into the γ' layer especially along the direction normal to the surface

due to the large gradient of nitrogen content and eventually form columnar grains. In the furnace-cooling process after nitriding, γ' nitrides precipitate from ϵ grains due to the existence of nitrogen gradients in the ϵ layer and the modification of equilibrium ϵ phase with changing temperature, which results in a lamellar microstructure of a columnar compound layer. The γ' equiaxed grains under the columnar layer remain as a transition compound layer after cooling. In the zone under the transition layer where nitrogen dissolved and became supersaturated during cooling, γ' and α'' nitrides precipitate from the α substrate (nitrogen ferrite) and form the diffusion layer ($\gamma' + \alpha'' + \alpha$). The cross-sectional micrograph of the nitrided pure iron in this work is similar to that of nitrided iron steels reported previously.^{9,11} The nitrided layers have thickness of up to 1 mm, consisting of a top columnar layer (9–10 μm), middle transition layer (3–5 μm), and diffusion layer (balance). Figure 1 shows the nitrogen depth profile observed by electron beam probe analyzer. The nitrogen concentration gradually decreases in the compound layer (about 15 μm in thickness) and then slightly fluctuates in the diffusion layer. The columnar and transition sublayers could not be distinguished according to this profile.

In nitrided pure iron layer, γ' nitrides were observed in both compound and diffusion layers. Due to different precipitation mechanisms, γ' nitrides have different morphologies in the columnar compound layer, transition compound layer, and diffusion layer. It was found that there were two kinds of γ' nitrides in the diffusion layer. One was full of parallel striations running through its body, while the other was not. To distinguish these two morphologies, they were tentatively named as striated γ' nitride and unstriated γ' nitride. Therefore, a total of four kinds of γ' nitrides were observed in the nitrided layer as shown in Fig. 2. The microstructures of the columnar compound layer [Fig. 2(a)] and transition compound layer [Fig. 2(b)] containing the γ' phase, and the morphologies of striated [Fig. 2(c)] and unstriated [Fig. 2(d)] γ' nitrides in the diffusion layer were presented, respectively.

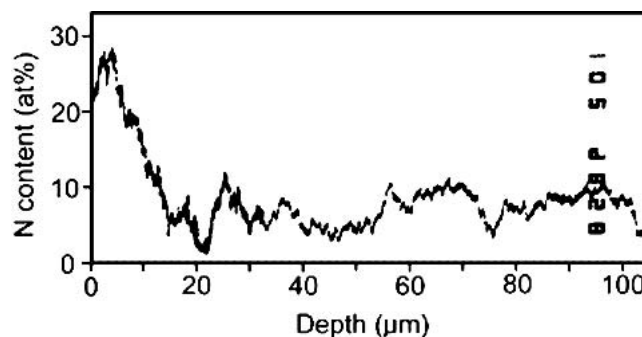


FIG. 1. Depth profile of nitrogen concentration measured by electron beam probe analyzer.

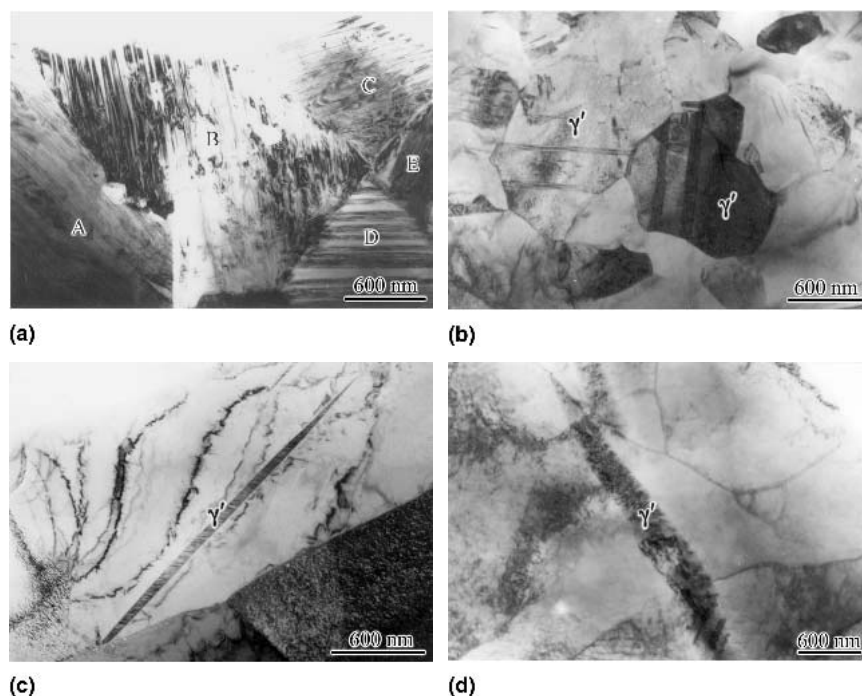


FIG. 2. Morphology of (a) lamellar structure in columnar compound layer, (b) equiaxed grains in transition compound layer, (c) striated, and (d) unstriated γ' nitrides in the diffusion layer.

A. γ' -Fe₄N nitride in the columnar compound layer

The columnar compound layer was made up of large grains, and each grain had a lamellar structure, in which parallel plates could be observed. Since the habit plane of the plate is fixed, the plate direction has something to do with the orientation of the grain. Therefore, different grains can be recognized easily according to the different directions of the plates as shown in Fig. 2(a), where five grains were indicated as A, B, C, D, and E. Figure 3 shows a HREM image of the $\epsilon + \gamma'$ lamellar structure in a columnar compound grain observed along the $[011]\gamma'//[1\bar{2}10]\epsilon$ orientation. From left to right, the plates are ϵ , γ' , ϵ , γ' , and ϵ , successively. It was shown that the lamellar structure of columnar grains resulted from alternating ϵ and γ' plates. According to the different HREM image configurations shown in the middle ϵ plate, it was concluded that ϵ' nitride with a superstructure was formed due to the ordering of nitrogen atoms in the ϵ plate.¹⁵ The different contrast in ϵ plate, especially those near the interface between γ' and ϵ plates, was coming from the local fluctuation of nitrogen concentration, which was reported being up to ± 8 at.% in ϵ nitride.¹⁶ The corresponding electron diffraction pattern of the image in Fig. 3 was inserted in the bottom left corner. This diffraction pattern contains one set of ϵ spots (left unit) and two sets of γ' spots (right units) with a twin relationship, which were indexed with four indices (ϵ) and three

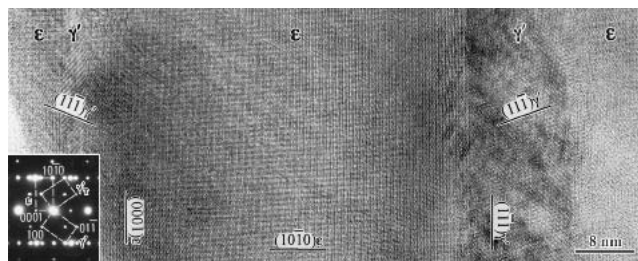


FIG. 3. HREM image of the lamellar structure constructed by ϵ and γ' plates viewed along $[011]\gamma'//[1\bar{2}10]\epsilon$ orientation. The inset shows the corresponding electron diffraction pattern.

indices (γ'), respectively. The orientation relationship between them is $(1\bar{1}1)\gamma'//(0001)\epsilon$, $[011]\gamma'//[1\bar{2}10]\epsilon$. Although the twin relationship of γ' was often detected during electron diffraction investigation of this $\epsilon + \gamma'$ lamellar structure, it was found during HREM observation that the twin relationship only occurred between two separate γ' plates but not within a single γ' plate as shown in Fig. 3, in which two γ' plates show a twin relationship with each other. Results from the diffraction analyses show that the plate habit plane of γ' is $\{1\bar{1}1\}\gamma'$ and that of ϵ is the $(0001)\epsilon$ plane. It was determined that the relatively thick plates were ϵ nitrides with a thickness of 25–115 nm and the thin γ' plates had a thickness of 3–12 nm in the columnar grains. It is necessary to point out that the thickness of the plates must be measured in the edge-on position. In other words, the orientation must be parallel to the

precipitate habit plane of $(1\bar{1}1)\gamma'$ or the $(0001)\epsilon$ plane as shown in the inset of Fig. 3, which is along the $[011]\gamma'//[1\bar{2}10]\epsilon$ orientation.

Figure 4 shows a HREM image of the interface between γ' and ϵ plates. Two interfaces were marked with horizontal dashed lines in the image. A ledge of γ' was observed on the upper interface with the steps two atomic layers high. A 60 atomic layer wide area of γ' between inclined solid black lines was analyzed carefully as indicated in Fig. 4. The corresponding atomic layers in the lower ϵ plate were also 60 layers, and those in the upper ϵ plate were only 59 layers. Three dislocations were indicated near the upper interface, whose extra planes were marked with dots. It is obvious that dislocation B was inside the γ' plate, while dislocations A and C were interfacial dislocations associated with the interfacial steps. According to topological theory,^{17,18} these interfacial dislocations were defined as $(b,h) = (1/6[2\bar{1}1]\gamma', 2d(1\bar{1}1)\gamma')$ noticing that the $1/6[2\bar{1}1]\gamma'$ dislocation is equivalent with the $1/3[10\bar{1}0]\epsilon$ dislocation. At the interface without interfacial steps (or ledges) between ϵ and γ' plates, no misfit dislocations were observed as shown in Figs. 3 and 4, indicating that the planar interface between ϵ and γ' is coherent. Although the lattice parameter of γ' nitrides depends on the nitrogen content,¹⁹ since its nitrogen concentration range is small in the iron nitrogen phase diagram,²⁰ the lattice parameter varies in a small range in the published works.^{21,22} Using the lattice constants of γ' ($a = 0.3795$ nm) given by Jack,¹² lattice parameters of ϵ in the columnar grain were calculated as $a = 0.268$ nm and $c = 0.438$ nm according to the $\epsilon + \gamma'$ diffraction pattern in the inset of Fig. 3. Therefore, the planar mismatch between $(10\bar{1}0)\epsilon$ and $(1\bar{1}1)\gamma'$ perpendicular to the interface is calculated as 0.17%. The coherent interface between these two phases indicates that the plane mismatch is fully accommodated by the elastic strain of the crystal lattice, which is believed to be

contained mainly in the elastically softer γ' side of the interface. This was verified by the fact that dislocations were observed in γ' plates but no dislocations were found in ϵ plates (see Figs. 3 and 4).

It is known that ϵ columnar grains form on the surface of samples during nitriding at high temperature. In the cooling process after nitriding, γ' plates precipitate from ϵ grains by virtue of $\epsilon \rightarrow \gamma'$ phase transformation. Some γ' plates ended within ϵ grains, indicating that the grain boundaries of primary ϵ grains are preferred places for nucleation of γ' plates. During the nucleation and formation of γ' (fcc structure) plates at primary ϵ (hcp structure) grain boundaries, structural change from hcp to fcc is needed. According to the orientation relationship between γ' and ϵ plates as shown in Fig. 3, both close-packed planes and close-packed directions in these two structures are parallel with each other. Therefore, the transformation from ϵ to γ' could occur by slip of $1/3[10\bar{1}0]\epsilon$ partial dislocations in every successive $(0001)\epsilon$ plane. If such slip takes place in two successive $(0001)\epsilon$ planes, a twin structure will be obtained, which is consistent with the observation among γ' plates. Since the nitrogen concentration range of γ' nitrides (± 0.5 at.%) is narrower than that of ϵ nitrides (± 8 at.%), the precipitated γ' plates have smaller thickness than that of ϵ plates.¹⁶ The above transformation model was verified by the observations of interfacial steps along the interface between ϵ and γ' plates as shown in Fig. 4. It is obvious that the $\epsilon \rightarrow \gamma'$ nitride transformation in the columnar compound layer is a displacive–diffusive transformation, which exhibits the crystallographic features of a martensitic process. Its mechanism is the typical one in the transformation between hcp and fcc crystal structures, which is also applied in TiAl^{23–26} and other alloys.^{27,28}

B. γ' -Fe₄N nitride in the transition compound layer

The transition compound layer was under the surface columnar compound layer and was made up of small equiaxed grains with a size of 1–1.5 μm as shown in Fig. 2(b). It was observed that most of the grains were γ' nitrides, among which ϵ grains could also be observed. The stacking faults and twins were often observed in this kind of γ' equiaxed grains. In addition to the typical $\{111\}\gamma'$ twin, a $\{112\}\gamma'$ twin was also observed in γ' equiaxed grains. The mixture of these two type twins gave a steplike morphology as shown in Fig. 5. Parts A–B, C–D, E–F, and G–H are $(1\bar{1}1)\gamma'$ twin boundaries, while parts B–C, D–E, F–G, and H–I are $(2\bar{1}1)\gamma'$ twin boundaries. Linear contrast, which is parallel to the $(1\bar{1}1)\gamma'$ twin boundary, could be observed on the $(2\bar{1}1)\gamma'$ twin boundary, especially on part I in Fig. 5, as indicated by arrow heads. This linear contrast existed on both sides of $(2\bar{1}1)\gamma'$ twin boundaries with a small displacement. Its

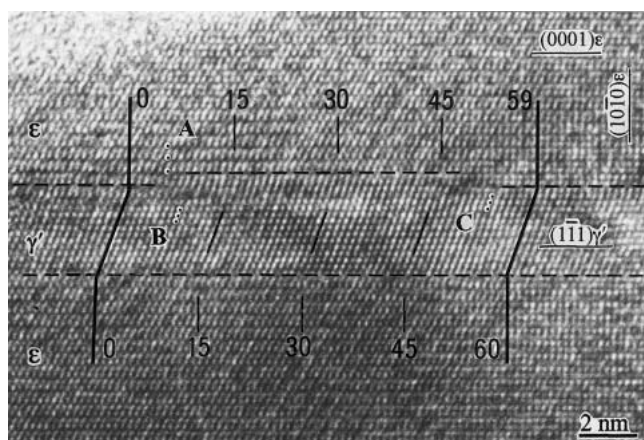


FIG. 4. HREM image of the interface between ϵ and γ' plates in columnar compound layer with a ledge on the upper interface.

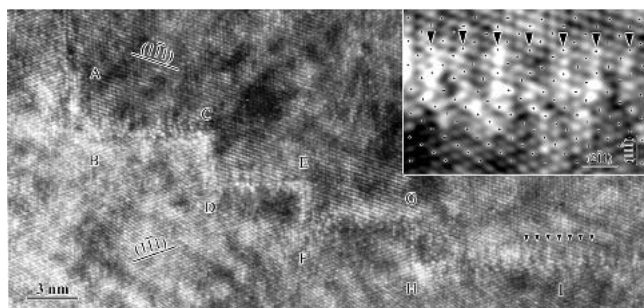


FIG. 5. The $\{11\bar{1}\}\gamma'$ and $\{2\bar{1}1\}\gamma'$ twin boundary steps in γ' equiaxed grain. The inset is an enlarged image of part I after Fourier transform filtering, in which only atoms in one layer viewed along $[011]\gamma'$ orientation were marked with black dots.

average spacing was measured as 0.67 nm, which is almost three times the spacing of the $(11\bar{1})\gamma'$ planes (0.2191 nm). It is believed that a dislocation with Burgers vector of about $1/9[11\bar{1}]\gamma'$ exists at the junction of the $(11\bar{1})\gamma'$ and $(2\bar{1}1)\gamma'$ twin boundaries, resulting in distortion of the $(11\bar{1})\gamma'$ planes to which the Burgers vector is perpendicular.²⁹ The magnified $(2\bar{1}1)\gamma'$ twin boundary around part I was subjected to Fourier transform filtering to eliminate noise, and a magnified view is shown in the inset. Only one layer of the atoms viewed along the $[011]\gamma'$ orientation was marked by black spots, from which the atomic arrangement of the twin boundary can be seen.

Unlike the γ' plates in the columnar compound layer, above γ' equiaxed grains were formed at high temperature during nitriding and then remained as a transition compound layer after cooling to room temperature. Therefore, stacking faults and twin boundaries could be generated in the nucleation and grown process.

C. γ' -Fe₄N nitride with striations in the diffusion layer

One kind of γ' nitride in the diffusion layer had a lenticular morphology with fine parallel striations inside, as shown in Fig. 2(c). A HREM image of the interface between the γ' nitride and α substrate is shown in Fig. 6. It was observed that the fine parallel striations were stacking fault plates inside the γ' nitride, which produced streaks in the reciprocal lattice perpendicular to the fault planes as shown in the inset of Fig. 6. According to this diffraction pattern, the orientation relationship between γ' (top white unit) and α (bottom black unit) is $(100)\gamma'//[1\bar{1}0]\alpha$, $[011]\gamma'//[111]\alpha$. The stacking fault is the only crystal defect observed in this kind of γ' nitride, and its density is very high. They generated on only one set of $\{1\bar{1}1\}\gamma'$ planes, and most of them run through the cross section of nitride and ended at the interfaces, which results in the parallel characteristic at low magnification [see Fig. 2(c)]. Unlike the interface between ϵ and γ' plates in the columnar compound layer

(see Fig. 4), the interface between γ' nitride and α substrate is very complicated due to the formation of extensive stacking faults as shown in Fig. 6. The extra planes are marked with symbol “ \perp ” and the dislocations distributed on both sides of the interface. The interface between γ' and α was roughly determined as $(\bar{5}32)\alpha$ in Fig. 6.

This striated γ' nitride was observed to be divided into several parts due to the slide within the nitrides. Figure 7 shows a striated γ' nitride indicated by A, B, and C letters with the length of about 8 μm . Its left end (part A) shows a typical needlelike profile as that in Fig. 2(c). Part B–C of this nitride is shown in Fig. 7(b), in which the sliding trace can be seen as indicated by arrows. In part D it seems that the sliding between left and right parts just took place, while in parts E and F the γ' nitride has broken into several parts that even separated from each other. Since Fig. 7 was observed along the $[011]\gamma'$ orientation where two sets of $\{111\}\gamma'$ planes can be viewed edge-on, it is interesting to find that the slide took place on the other set of the $\{111\}\gamma'$ plane without parallel stacking faults. This phenomenon was only observed in large γ' (the length is over 6 μm). In small γ' nitride as shown in Fig. 2(c), no sliding trace was found. It is deduced that the sliding on the $\{111\}\gamma'$ plane without parallel stacking faults will release the accumulated strain produced by highly dense parallel stacking faults in one direction, and the stability of γ' is improved.

It was noticed that part C of the γ' nitride in Fig. 7(a) was connecting with an α'' -Fe₁₆N₂ nitride directly, which gives evidence for the transformation from α'' to γ' nitride. It was concluded that the precipitation of striated γ' comes from the $\alpha'' \rightarrow \gamma'$ nitride transformation, during which $[110]\alpha''$, $[1\bar{1}0]\alpha''$, and $[001]\alpha''$ axes

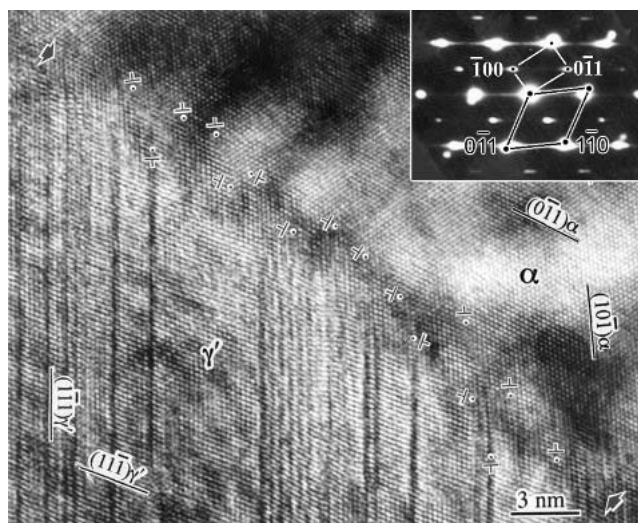


FIG. 6. HREM image of interface between striated γ' nitride and α substrate viewed along $[011]\gamma'//[111]\alpha$ orientation with corresponding diffraction pattern (see the inset).

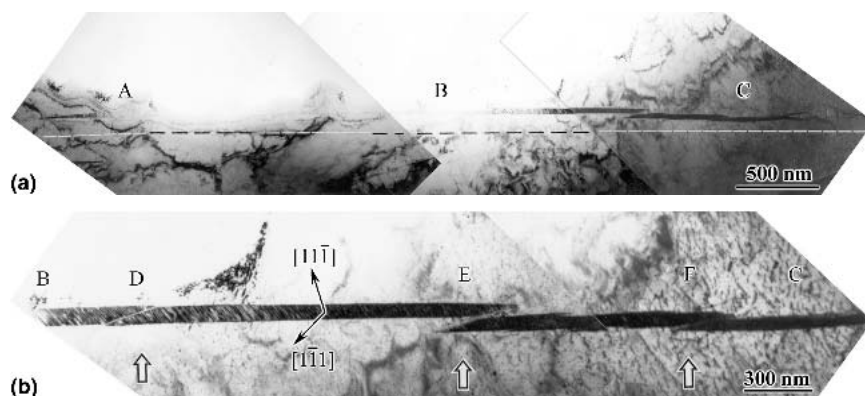


FIG. 7. Morphology of (a) a striated γ' nitride and (b) its magnified image of part B–C viewed along the $[011]\gamma'$ orientation. Stacking faults existed on the $(1\bar{1}1)$ plane while the sliding took place on $\{11\bar{1}\}\gamma'$ plane (see parts D, E, and F).

transformed to $[100]\gamma'$, $[001]\gamma'$, and $[010]\gamma'$ axes, respectively.³⁰ With lattice parameters of α'' nitride ($a = 0.572$ nm, $c = 0.627$ nm)³⁰ and γ' nitride ($a = 0.3795$ nm),¹² the misfit degree along each axis pair mentioned above is calculated as 6.43%, 6.43%, and 18.73%, respectively, noticing that the misfit degree between $(001)\alpha''$ and $(010)\gamma'$ is very high (18.73%). It was speculated that the high misfit degree (18.73%) in this transformation can only be accommodated by highly dense oriented planar faults, which results in the fine parallel striations in γ' . Both the α'' nitride and the remaining α'' lattice after dissolution could act as the preferred sites for the nucleation of γ' nitride. Since the orientation relationship between γ' and α'' is $(100)\gamma' // (1\bar{1}0)\alpha''$ $[011]\gamma' // [111]\alpha$ and a parallel orientation relationship exists between α'' and α substrates^{30–32} the orientation relationship between γ' and α should be $(100)\gamma' // (1\bar{1}0)\alpha$ $[011]\gamma' // [111]\alpha$. This was verified by the observed diffraction pattern as shown in the inset of Fig. 6.

D. γ' -Fe₄N nitride without striations in the diffusion layer

In addition to the γ' with fine striations, another kind of γ' nitride without parallel striations was also observed as shown in Fig. 2(d). The morphology of this unstriated γ' is similar to the striated one with needlelike tips, but its body was large and not straight [see Fig. 2(d)]. A HREM image of this unstriated γ' is shown in Fig. 8 together with the inserted corresponding $[001]\gamma'$ diffraction pattern. Compared with the striated γ' in Fig. 6, no striations were observed in Fig. 8 and the corresponding elongated streaks also disappeared in the diffraction pattern. Although the stacking faults also existed in this kind of γ' as indicated by arrows in Fig. 8, these stacking faults were short and on both sets of $\{111\}\gamma'$ planes without preference. It was observed that the microstructure of this unstriated γ' nitride was very complicated due to the dislocations, stacking faults, low-angle grain boundaries, and misoriented grains. Figure 9 shows a

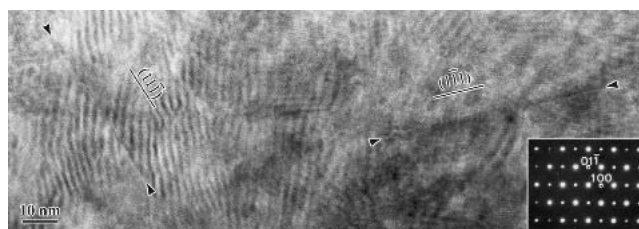


FIG. 8. HREM image of small stacking faults generated on different sets of $\{111\}\gamma'$ planes in γ' nitride without striations. The inset shows the corresponding $[011]\gamma'$ diffraction pattern.

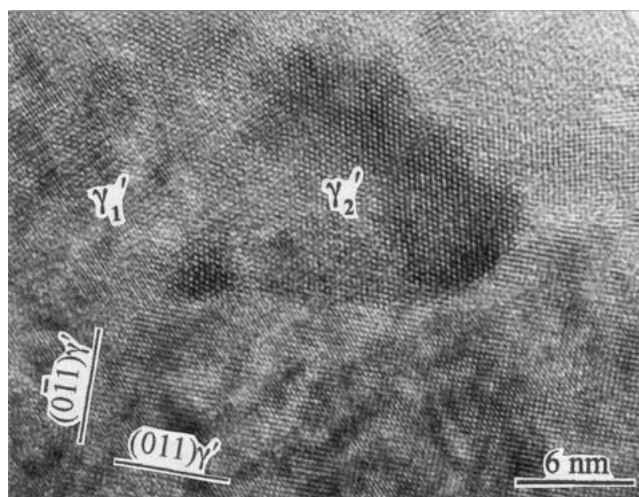


FIG. 9. HREM image of a misoriented grain in an unstriated γ' nitride. The matrix (γ_1') was viewed along the $[100]\gamma'$ orientation while the γ_2' grain is in $[111]\gamma'$ orientation.

HREM image observed along $[001]\gamma'$ orientation, in which a small misoriented triangle $[111]\gamma'$ grain with dark contrast was observed.

It is obvious that the precipitation characteristic of this unstriated γ' nitride is different from those striated γ' nitrides. The $\alpha'' \rightarrow \gamma'$ direct transformation discussed in Sec. C was not detected on this kind of γ' without striations. It is reasonable to believe that unstriated γ' nitrides

nucleated from nitrogen-rich substrate areas with the orientation relationship of $(100)\gamma'//(\bar{1}\bar{1}0)\alpha$ $[011]\gamma'//[111]\alpha$, which has been described in the inset of Fig. 6 and reported by others.^{8,33} According to this orientation relationship, the misfit degree between $\{010\}\gamma'$ and $\{110\}\alpha$ planes is only 6.57%. This degree is homogeneous and lower than the average degree in the $\alpha'' \rightarrow \gamma'$ transformation (see Sec. C); thus, the small stacking faults could be generated on different sets of $\{111\}\gamma'$ planes without preference. Since little information was reported on this kind of γ' hitherto, more efforts should be made to clarify its precipitation mechanism.

IV. CONCLUSIONS

(1) Four kinds of γ' -Fe₄N nitrides with different morphologies and microstructures were formed in the nitrided layer of polycrystalline pure iron due to different precipitation mechanisms.

(2) In the columnar compound layer γ' plates precipitated from ϵ -Fe₂₋₃N columnar grains with orientation relationship of $(\bar{1}\bar{1}1)\gamma'//(0001)\epsilon$ and $[011]\gamma'//[1\bar{2}10]\epsilon$, and resulted in a lamellar structure in the grain. HREM observation indicates that γ' plates (3–12-nm thickness) and ϵ plates (25–115-nm thickness) array alternatively in each lamellar grain and a twin relationship only occurs between different γ' plates. In spite of interfacial steps, the planar interface between ϵ and γ' plates is coherent.

(3) The γ' nitrides in the transition compound layer appeared as equiaxed grains (1–1.5 μm), which nucleated and grew from α -Fe substrate during nitriding at high temperature and then were maintained in the following cooling process.

(4) In the diffusion layer, the lenticular γ' with parallel striations was fully filled with a high density of stacking faults generated on only one set of $\{111\}\gamma'$ plane. This striated γ' nitride precipitated from the α'' -Fe₁₆N₂ lattice with the orientation relationship of $(100)\gamma'//(\bar{1}\bar{1}0)\alpha''$ and $[011]\gamma'//[111]\alpha''$. The sliding took place on the other set of $\{111\}\gamma'$ plane without stacking faults, which divided the nitride into several parts.

(5) The unstriated γ' nitrides in the diffusion layer also had lenticular morphology and precipitated from the α substrate with orientation relationship of $(100)\gamma'//(\bar{1}\bar{1}0)\alpha$ and $[011]\gamma'//[111]\alpha$. The short stacking faults on different sets of $\{111\}\gamma'$ planes and a misoriented grain were observed with HREM.

ACKNOWLEDGMENTS

The authors give grateful thanks to Mr. J.X. Wang (Institute of Materials and Technology, Dalian Maritime University, Dalian, China) for nitriding the specimens

used in this study. The financial support from the National Natural Science Foundation of China (Grant No. 50071063) is also appreciated.

REFERENCES

1. T. Bell, *Heat Treat. Met.* **2**, 39 (1975).
2. K. Sachs and D.B. Clayton, *Heat Treat. Met.* **6**, 29 (1979).
3. D.L. Guan and Z.W. Yu, in *Mechanical Behaviour of Materials—VI*, edited by M. Jono and T. Inoue (Pergamon Press, Elmsford, New York, 1991), p. 295.
4. M.K. Lei and Z.L. Zhang, *J. Mater. Sci. Lett.* **16**, 1567 (1997).
5. G.B. Li, G.Q. Li, M.K. Lei, and B.Z. Liu, *Surf. Coat. Technol.* **96**, 34 (1997).
6. G.R. Booker, J. Norbury, and A.L. Sutton, *Journal of the Iron and Steel Institute* **187**, 205 (1957).
7. D. Gerardin, J.P. Morniroli, H. Michel, and M. Gantois, *J. Mater. Sci.* **16**, 159 (1981).
8. D. Gerardin, H. Michel, J.P. Morniroli, and M. Gantois, *Mem. Sci. Rev. Metall.* **74**, 457 (1977).
9. X.L. Xu, L. Wang, Z.W. Yu, and Z.K. Hei, *Metall. Mater. Trans. A* **27**, 1347 (1996).
10. J. D'Haen, C. Quaeysaegens, G. Knuyt, M. D'Olieslaeger, and L.M. Stals, *Surf. Coat. Technol.* **74–75**, 405 (1995).
11. X.L. Xu, L. Wang, Z.W. Yu, and Z.K. Hei, *Acta Metall. Sin. (Engl. Lett.)* **11**, 183 (1998).
12. K.H. Jack, *Proc. R. Soc. A* **195**, 34 (1948).
13. G.R. Booker, *Acta Metall.* **9**, 590 (1961).
14. U. Dahmen, P. Ferguson, and K.H. Westmacott, *Acta Metall.* **35**, 1037 (1987).
15. Z.Q. Liu, D.X. Li, Z.K. Hei, and H. Hashimoto, *Scr. Mater.* **45**, 455 (2001).
16. M.A.J. Somers and E.J. Mittemeijer, *Metall. Mater. Trans. A* **26**, 57 (1995).
17. J.P. Hirth and R.C. Pond, *Acta Mater.* **44**, 4749 (1996).
18. R.C. Pond, P. Shang, T.T. Cheng, and M. Aindow, *Acta Mater.* **48**, 1047 (2000).
19. M.A.J. Somers, N.M. van der Pers, D. Schalkoord, and E.J. Mittemeijer, *Metall. Mater. Trans. A* **20**, 1533 (1989).
20. K.H. Jack, *Proc. R. Soc. A* **208**, 200 (1951).
21. G. Hagg, *Z. Phys. Chem.* **8**, 455 (1930).
22. B. Rauschenbach, A. Koliutsch, and K. Hohmuth, *Phys. Status Solidi A* **80**, 471 (1983).
23. G.J. Mahon and J.M. Howe, *Metall. Trans. A* **21**, 1655 (1990).
24. P. Shang, T.T. Cheng, and M. Aindow, *Philos. Mag. A* **79**, 2553 (1999).
25. X.W. Du, J. Zhu, X. Zhang, Z.Y. Cheng, and Y.W. Kim, *Scr. Mater.* **43**, 597 (2000).
26. K. Hashimoto, M. Kimura, and Y. Mizuhara, *Intermetallics* **6**, 667 (1998).
27. J.M. Howe, U. Dahmen, and R. Gronsky, *Philos. Mag. A* **56**, 31 (1987).
28. H.S. Fang and C.M. Li, *Metall. Trans. A* **25**, 2615 (1994).
29. W. Krakow and D.A. Smith, *Ultramicroscopy* **22**, 47 (1987).
30. Z.Q. Liu, Y.X. Chen, Z.K. Hei, D.X. Li, and H. Hashimoto, *Metall. Mater. Trans. A* **32**, 2681 (2001).
31. Z.Q. Liu, X.L. Xu, Z.K. Hei, R.N. Guan, R.S. Li, and D.X. Li, *Acta Metall. Sin. A* **36**, 7 (2000).
32. Z.Q. Liu, D.X. Li, X.L. Xu, L. Wang, and Z.K. Hei, *J. Mater. Sci. Technol.* **16**, 362 (2000).
33. G. Hinojosa, J. Oseguera, and P.S. Schabes-Retchkiman, *Thin Solid Films* **349**, 171 (1999).